Electrochimica Acta 292 (2018) 697–706

Contents lists available at ScienceDirect

Electrochimica Acta

journal homepage: www.elsevier.com/locate/electacta

Perovskite solar cells with versatile electropolymerized fullerene as electron extraction layer

María B. Suárez [a], Clara Aranda [b], Lorena Macor [a], Javier Durantini [a], Daniel A. Heredia [a], Edgardo N. Durantini [a], Luis Otero [a], Antonio Guerrero [b, **], Miguel Gervaldo [a, *]

[a] Departamento de Química, Universidad Nacional de Río Cuarto, IITEMA-IDAS-CONICET Agencia, Postal Nro. 3, X5804BYA, Río Cuarto, Córdoba, Argentina
[b] Institute of Advanced Materials (INAM), Universitat Jaume I, 12006, Castelló, Spain

ARTICLE INFO

Article history:
Received 2 May 2018
Received in revised form
12 September 2018
Accepted 29 September 2018
Available online 2 October 2018

Keywords:
Perovskite
Electropolymerization
Fullerene electropolymer
Electron transport material
Photoluminescence quenching

ABSTRACT

An electropolymerized layer of a C_{60} fullerene derivative was successfully used as selective contact and electron transport layer in perovskite solar cells. The electropolymeric film was formed over FTO electrodes by an electrochemical methodology in just one step. The light emission of perovskite films formed over the electropolymer was quenched, confirming an efficient electron transfer from the perovskite to the electropolymerized C_{60} layer. Solar cells constructed with C_{60} polymer layer showed a much better performance compared with the same cell without the fullerene containing electropolymer layer. The best non-optimized device presented an efficiency of 11.0%, with an open circuit voltage of 969 mV, a short circuit current of 17 mA/cm^2, and a fill factor of 65%. These results demonstrated that the use of an electrochemical methodology in the formation of an organic electron transport layers as replacement of metal oxides in perovskite solar cells opens a new approach in the fabrication of efficient energy conversion systems.

1. Introduction

Solar cells based on hybrid organic-inorganic materials with perovskite (PS) crystallographic structure have attracted extensive attention that has exponentially grown since their first introduction in 2009 [1–4]. The "new wave" of this emerging technology [5] has been motivated by the potential to obtain efficient and cost-effective solar energy conversion devices [6]. Metal-halide ABX_3 perovskite based solar cells can be classified into mesoscopic (MHJ) and planar heterojunction (PHJ) configurations [7–9]. In MHJ devices the perovskite is formed onto a scaffold that is prepared under high temperature conditions, usually above 450 °C, and composed typically by nanostructured titanium, aluminum or zinc oxide [8,9]. On the contrary, in the PHJ configuration the metal-halide perovskite active layer is sandwiched between two planar charge selective contacts [10–12]. In this respect, for the development of efficient and stable PHJ devices, the hole extraction and transport layers (HTL), and the electron extraction and transport layers (ETL) need to fulfill a range of stringent requirements, including an adequate energy level alignment [13]. In general, PHJ solar cells are less efficient than the mesoscopic counterpart but their performances are approaching [14]. On the other hand, the PHJ configuration simplifies the fabrication process in comparison with MHJ, avoiding the use of a high temperature step for the sintering of the mesoporous metal oxides. Thus, low temperature methods allow the fabrication of large area and flexible perovskite solar cells, using techniques compatible with industrial requirements [15].

Several ETL have been used in perovskite based solar cells with chemical structures derived from those used in organic solar cells [16]. In this frame, in planar and mesoscopic perovskite solar cells [17–19], C_{60} fullerene has shown to be a strong electron acceptor useful not only as selective contact, but also as passivation agent for the charge traps at the grain boundaries of perovskite surface [20]. This effect largely reduces the current-voltage hysteresis in the device, and has increased the power conversion efficiency [21]. The material is typically deposited by spin coating either on the top of the perovskite or on a transparent conductive substrate as thin layer of about 20–50 nm [22]. Unfortunately, spin coating is not compatible with industrial production requirements, and for the

* Corresponding author.
** Corresponding author.
E-mail addresses: aguerrero@uji.es (A. Guerrero), mgervaldo@exa.unrc.edu.ar (M. Gervaldo).

https://doi.org/10.1016/j.electacta.2018.09.196
0013-4686/

manufacture of large areas devices. In addition, in various reports the fullerene is introduced between a compact or nanostructured oxide layer and perovskite film, which precludes the advantage of avoiding high temperature steps [23]. Also, the presence of a metallic oxide catalytic surface can induce device photodegradation [24]. Furthermore, until now discrete fullerene molecules have been used mostly with no chemical bonds involved in the layers generation, which could be useful to lock the film morphology and to reduce fullerene solubility against subsequent processing solvents. For this reason, fullerene layers can unintentionally be dissolved during perovskite layer deposition or during addition of the HTL layer by percolation from the edge of the perovskite layer or *via* pinholes. In order to avoid dissolution of the fullerene layer Wojciechowski et al. [19] showed that insoluble films could be obtained by the use of cross-linking units, improving in this way the *n*-type charge collection contact with efficiencies in the range of 12–16%. However, spin coating was needed for deposition of fullerene and the crosslinker. More importantly, discrete fullerene materials frequently suffer aggregation during the lifetime of the device, affecting the long term stability [25]. Thus, the evolution of PHJ solar cells using fullerene based selective contacts requires the development of alternative methods to spin coating, whilst obtaining adequate efficiency and stability of the devices. As a new approach, in this work we use an electropolymerized layer of a C_{60} fullerene generated in one single step at room temperature, which showed relatively high efficiency and stability during device fabrication and illumination. Recently, Yan et al. [26,27] demonstrated in a pioneer work the use of electropolymerized organic films as HTLs in inverted perovskite solar cells with efficiencies in the range of 12–16%. The used methodology provides a practical way to obtain HTLs using large-scale production methods for efficient perovskite solar cells. It is necessary to point out that the HTL or ETL layers where the perovskite layer will be deposited need to possess high uniformity, high stability, and well-controlled thickness, all goals that can be reached by electrochemical polymer generation [28,29]. In addition, contrarily to thermal evaporation of organic materials used for the assembly of optoelectronic devices, electrochemical polymerization does not require expensive vacuum equipment and high running costs. Also, in comparison with low-cost solution processes (i.e. spin or dip coating) electrochemical polymeric film generation does not necessitate polymers with intrinsic high solubility, and does not produce large amounts of pollutant solvent waste.

In the present report we extend the use of electrochemical deposition of polymeric films for the production of ETLs by using 3,4-ethylenedioxythiophene (EDOT) units containing C_{60} pendant moieties as electron acceptors for PHJ perovskite solar cells. The new C_{60} monomer derivative was designed in order to allow its electropolymerization over conductive substrates (Fig. 1). The polymer containing C_{60} units was generated over FTO electrodes by a simple electrochemical methodology in one single step.

2. Experimental section

2.1. Materials

All materials were used as received. FTO glasses (25 × 25 mm, Pilkington TEC15, ~15 Ω/sq resistance), CH_3NH_3I (MAI, DYESOL), PbI_2 (TCI, 99.99%), Spiro-OMeTAD (Merck). The perovskite precursor solution was prepared by reacting DMF solutions (50 wt %) containing MAI and PbI_2 (1:1 mol %) and MAI, PbI_2 and DMSO (1:1:1 mol %). The spiro-OMeTAD solution was prepared by dissolving in 1 mL of chlorobenzene 72.3 mg of (2,2′,7,7′-tetrakis(*N*,*N*′-di-*p*-methoxyphenylamine)-9,9′-spirobifluorene), 28.8 μL of 4-*tert*-butylpyridine, and 17.5 μL of a stock solution of 520 mg/mL of lithium bis- (trifluoromethylsulfonyl) imide in acetonitrile.

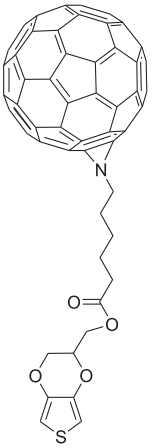

EDOT-C_{60}

Fig. 1. Chemical structure of EDOT-C_{60} monomer.

2.2. Device fabrication

All the process was carried out outside the glovebox in ambient conditions at relative humidity close to 35%. Photovoltaic devices were prepared over FTO glasses, which were partially etched with zinc powder and HCl (2 M). The substrates were cleaned with soap (Hellmanex) and rinsed with Milli-Q water and ethanol. Then, the substrates were sonicated for 15 min in a solution of acetone:isopropanol (1:1 v/v), rinsed with ethanol and Milli-Q water, and dried with compressed air. After that, the substrates were treated in a UV–O_3 chamber for 15 min. EDOT-C_{60} was obtained from fullerene C_{60} and (2,3-dihydrothieno[3,4-b] [1,4]dioxin-2-yl)methyl 6-azidohexanoate according with the procedure previously reported [30]. Poly-EDOT-C_{60} layers were fabricated on the cleaned mentioned FTO electrodes by cycling a 0.5 mM EDOT-C_{60} solution containing 0.1 M $TBAPF_6$ as support electrolyte in dichloroethane, in the −0.50–1.30 V vs SCE range. The electrochemical responses of the Poly-EDOT-C_{60} films were obtained in dichloroethane containing only support electrolyte. All measurements were carried out in a conventional three electrode cell, using a Pt counter electrode, an Ag wire as pseudoreference electrode, and Pt or FTO as working electrode. The potential axis was calibrated vs the formal potential for the Saturated Calomel Electrode (SCE), using Ferrocene as an internal standard.

The perovskite precursor solution (50 μL) was spin-coated at 4000 rpm for 50 s. DMF is selectively washed with non-polar diethyl ether while one-step spin-coating at 4000 rpm is carried out. After deposition, the substrate was annealed at 100 °C for 3 min. Then, the perovskite films were covered with the hole-transporting material (HTM) by dynamically spin coating at 4000 rpm for 30 s, using 50 μL of spiro-OMeTAD solution. Finally, 60 nm of gold was thermally evaporated on top of the device to form the electrode contacts using a commercial Univex 250 chamber, from Oerlikon Leybold Vacuum.

2.3. Film and device characterization

Ultraviolet–visible absorption spectra were recorded by a Cary 500 Scan VARIAN spectrophotometer in the 250–800 nm

wavelength range. Scanning electron microscopy (SEM) images were obtained with a field emission scanning electron microscope FE-SEM, Sigma Zeiss working at 3 kV. AFM images were recorded with a JSPM-5200 JEOL Scanning Probe Microscope. AFM images were obtained in contact mode using n-type silicon probes with a spring constant of ≈0.18 N/m and a typical resonance frequency of ≈13 kHz (HQ:CSC17/AL BS, MikroMasch). X-ray diffraction (XRD) patterns were obtained in a Philips PW1800/10 diffractometer operated at 40 kV and 30 mA with a Cu-Kα radiation source. Emission spectra were obtained with a spectrofluorometer (FluoroMax-4, Horiba). Photovoltaic devices were characterized using an Abet Solar simulator equipped with 1.5 AM filter. The light intensity was adjusted to 100 mWcm^{-2} using a calibrated Si solar cell. Devices were measured using a mask to define an active area of 0.11 cm^2. Devices were measured under reverse bias at a low 50 mV/s scan rate to minimize the effect of hysteresis. The polymer structure was obtained by the relaxation of all the atomic positions in a unit cell containing four EDOT-C_{60} monomers (a total of 316 atoms) to emulate the Poly-EDOT-C_{60} structure. The structure relaxation was obtained using molecular mechanics and force field calculations MMFF94s [31] as implemented in the Avogadro package [32]. The algorithm is based on a gradient descendant calculation to minimize the energy of the whole system, with an energy convergence value of 1×10^{-7} kJ/mol.

3. Results and discussion

3.1. Electrochemical polymeric film formation and characterization

Cyclic voltammetry was used in order to know the redox potentials of the monomer and to find the adequate conditions for electrochemical polymerization and film formation. Fig. 2a shows the first voltammetric scan of C_{60} monomer at a platinum electrode, where the cathodic and anodic processes are evidenced. An anodic current (which is not detected in a blank anodic scan) with an onset at around 1.20 V is observed, while in the cathodic direction two reduction peaks at −0.67 and −1.07 V are detected. The increasing anodic current and the cathodic peaks are assigned to oxidation of the EDOT units, and to the formation of the C_{60} radical anion and dianion respectively [30]. Cycling of the electrode in the monomer solution between −0.60 V and 1.3 V, conducts to increases in the oxidation-reduction currents after each new cycle, indicating the formation of an electroactive product adsorbed over the electrode surface (Fig. 2b) [33,34]. After five cycles, the electrode was removed from the monomer solution and placed in a solution containing only support electrolyte (see experimental section). The electrochemical responses of the film at different scan rates are shown in Fig. 2c. The film (called onwards as Poly-EDOT-C_{60}) shows anodic processes at around 0.10 and 1.2 V, and the corresponding complementary reduction process (peak at −0.46 V), typically found in the electrochemical response of PEDOT (Poly(3,4-ethylenedioxythiophene)) containing films [35]. On the other hand, two bell shaped cathodic peaks at −0.71 and −1.18 V, and their complementary reversible anodic processes are clearly distinguished. The cathodic peaks of Poly-EDOT-C_{60} occur at similar potentials than those observed for the monomer in solution, being possible to assign these two peaks to the first and second reduction of the C_{60} units. Also, the observed cathodic peaks confirm that the C_{60} units are still present in the film after the electropolymerization process, and retain their electrochemical properties. The anodic and cathodic peak currents present a lineal relation with the scan rate, typical of an electroactive product irreversibly adsorbed on the electrode surface [36]. It must be remarked that no film formation is observed if the scanned potential range does not include the anodic peak related to oxidation of the EDOT units. It has been demonstrated that oxidation of EDOT monomer conducts to the formation of PEDOT during anodic cycling [35]. The EDOT monomer was also electropolymerized on FTO electrodes in order to allow spectroscopic, morphologic and photovoltaic studies. The electrochemical responses of the polymeric films on FTO substrates were very similar to those obtained on Pt electrodes.

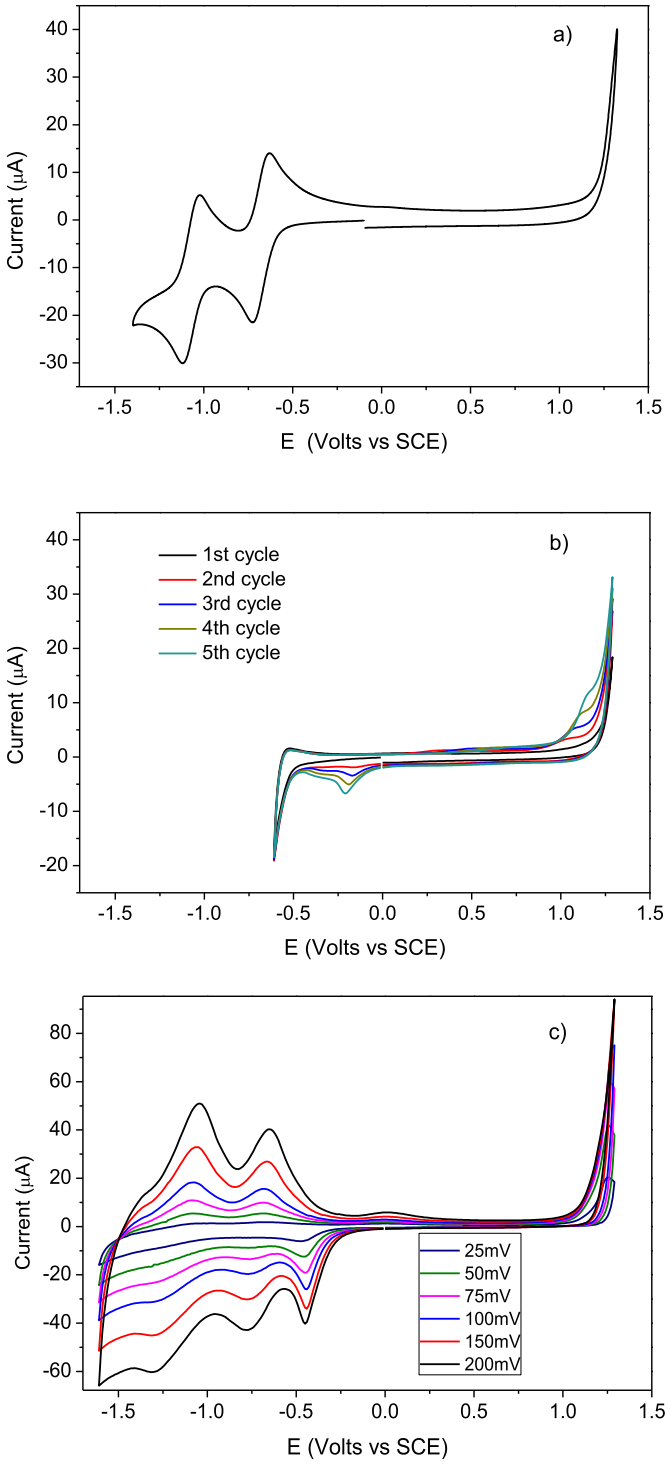

Fig. 2. a) First anodic and cathodic scan of EDOT-C_{60} monomer. b) Five consecutive cyclic voltammograms of EDOT-C_{60} monomer. c) Cyclic voltammograms at different scan rates of a Poly-EDOT-C_{60} film deposited on a Pt electrode.

3.2. AFM

Atomic Force Microscopy analysis (Fig. 3a) shows that the Poly-EDOT-C_{60} film presents a homogenous surface free of pinholes. The polymer topography closely follows the one observed for the FTO layer as it can be seen in Fig. 3b and c. In fact, the calculated roughness of the film (RMS = 3–5 nm) seems to be determined by the roughness of the FTO (RMS = 3–5 nm). This low roughness is very important in the posterior deposition of the perovskite layer, because rough surfaces could lead to the formation of pinholes and uneven films. It has been demonstrated that the use of electrochemical techniques with an appropriate control of the deposition parameters allows the formation of homogenous and pinhole free organic polymeric films with low roughness values [34,37,38]. Also, electrogenerated films have successfully been used as selective contact in perovskite solar cells with good efficiencies [26,27,39].

3.3. UV–vis spectroscopy

The transmission spectra of Poly-EDOT-C_{60} films show that these are semitransparent with bands at 330, 390, 470, and 630 nm (Fig. 4a). The intensity of all these bands increases with the number of polymerization cycles, indicating that the films become thicker with every new polymerization cyclic scan. From Fig. 4b the semitransparency and the increase in the intensity of the absorption bands of Poly-EDOT-C_{60} films can be clearly seen These bands are assigned to electronic transitions due to the presence of C_{60} aggregates in the films, as it has been previously reported for C_{60} layers deposited by physical vapor deposition [40–42]. On the other hand, after formation of perovskite films on top of the different Poly-EDOT-C_{60} layers the electrodes show a transmission close to 0 in the range 300–800 nm (Fig. 4a), with an on-set at 788 nm (measured at Abs = 0 by extrapolating the linear part of the absorption profile [43,44]), which corresponds to a band gap of 1.57 eV, typical of $CH_3NH_3PbI_3$ perovskites. These results demonstrate that Poly-EDOT-C_{60} thin films deposited over FTO semitransparent electrodes do not interfere in the PS light harvesting processes.

Taking into account the electrochemical and spectroscopic data, a polymer structure where the fullerene units are hanging from the PEDOT backbone is proposed (Fig. 5a). Molecular mechanics and force fields calculations were used to obtain more information about the spatial geometry of the polymer (see experimental section for details). Fig. 5b shows a three-dimensional structure, where it can be seen that the EDOT units are connected one to the other forming the principal backbone, while the fullerenes attached to these EDOTs are pointing out to opposite directions. Also due to the steric hindrance between adjacent fullerenes, these are twisted by 90° every two EDOT units. As a result a “helix” type polymer is formed.

3.4. Perovskite film formation and characterization

$CH_3NH_3PbI_3$ perovskite films were deposited over naked FTO and over FTO/Poly-EDOT-C_{60} electrodes by the methodology described in the experimental section. Fig. 6a shows SEM images with different magnification scales of PS films deposited over FTO, and FTO/Poly-EDOT-C_{60} substrates. As it can be seen, both films are almost indistinguishable with a very similar morphology, which consist of grains with sizes ranging from 100 to 400 nm. Also both surfaces are very homogeneous and uniform, without pinholes or cracks.

Fig. 6b shows a cross-section SEM image of a full device fabricated with Poly-EDOT-C_{60} (five polymerization cycles of EDOT-C_{60} monomer), which can be seen as a very thin dark layer with a

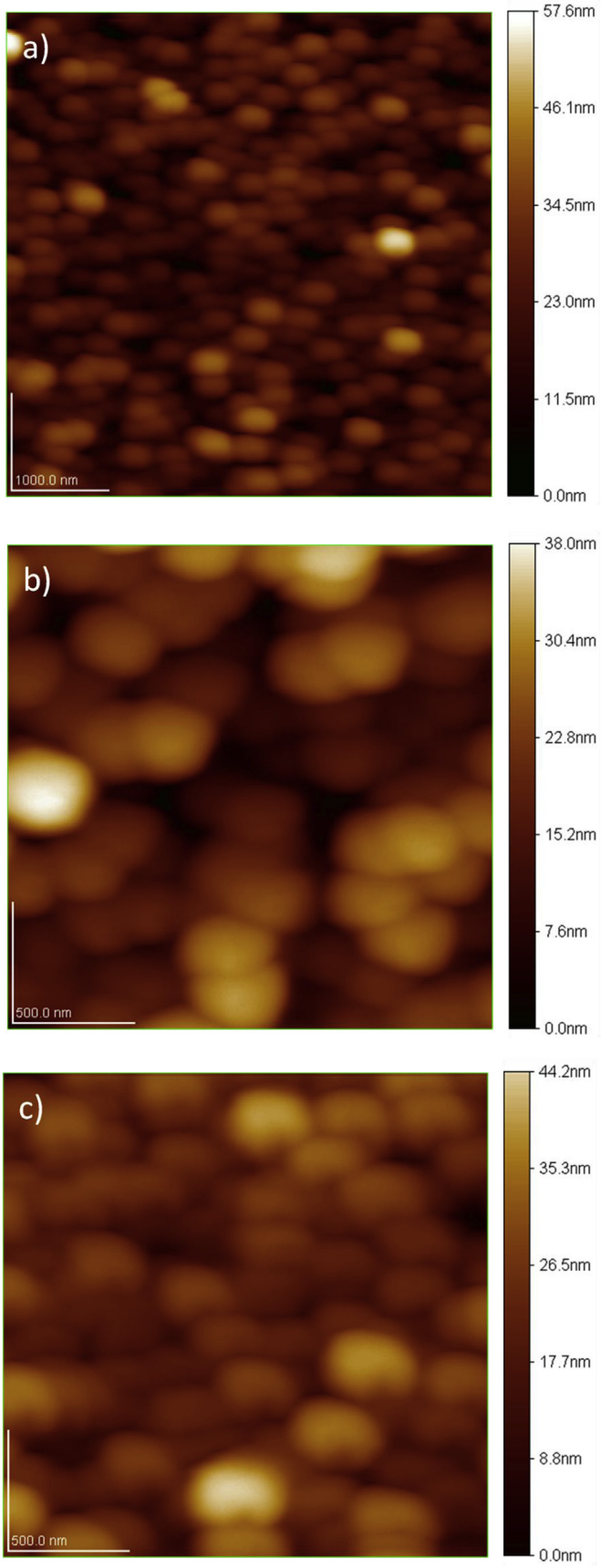

Fig. 3. a) AFM Topography image of Poly-EDOT-C_{60} film deposited on a FTO substrate (5 μm × 5 μm). b) Naked FTO substrate (2 μm × 2 μm). c) FTO/Poly-EDOT-C_{60} (2 μm × 2 μm). Images obtained by Atomic Force Microscopy working in contact mode (512 × 512 pixels, imaging speed: 1 line/s).

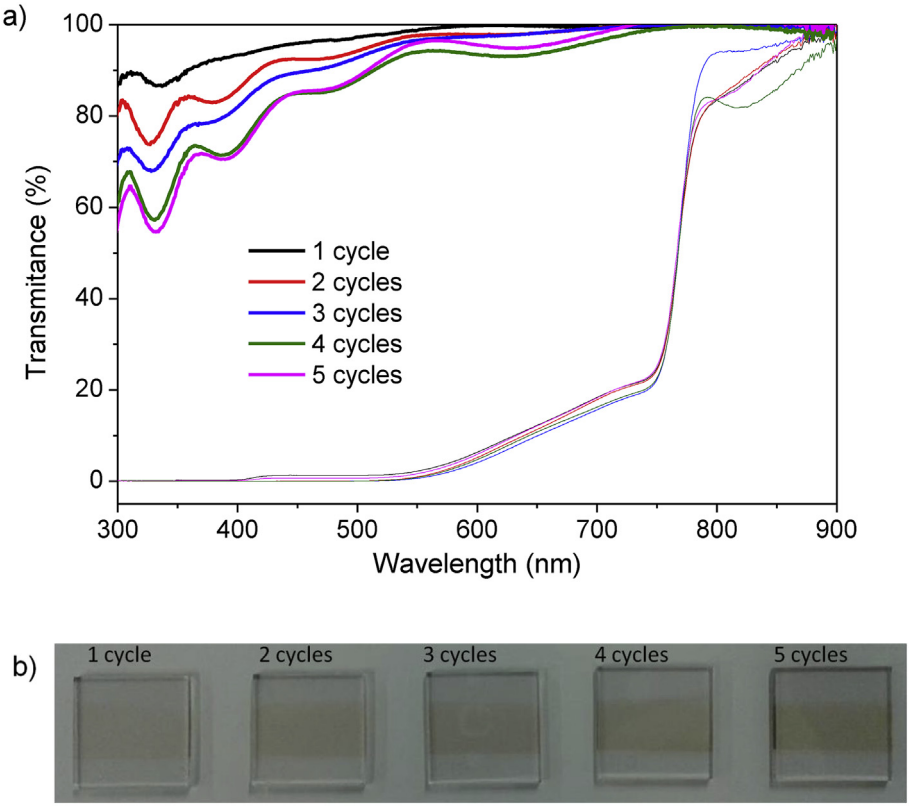

Fig. 4. a) Transmission spectra of electropolymerized films of Poly-EDOT-C_{60} on FTO electrodes (thick lines), and transmission spectra of perovskite films deposited on top of Poly-EDOT-C_{60} polymer (thin lines). b) Photographic images of films obtained by different number of polymerization cycles.

thickness of about 20 nm on the top of the FTO. Also, a thickness of around 300 nm is determined for the PS layer.

XRD was used to study the effect of the Poly-EDOT-C_{60} layer on the PS formation and phase composition. Fig. 7 shows a XDR diffractogram of PS deposited over FTO (top). The diffractogram presents peaks at 14.2°, 28.4°, 31.9°, 40.6°, and 43.2°, which are consistent with the (110), (220), (310), (224), and (314) planes of tetragonal $CH_3NH_3PbI_3$ phase [26,45–47]. Also minor peaks at 2θ values of 19.9°, 23.5°, 24.5°, 34.9°, 50.2°, and 52.5° associated to planes (226), (200), (211), (202), (312), (404), (226), and related also to tetragonal $CH_3NH_3PbI_3$ phase, clearly indicate that the perovskite film is high phase purity. When the PS is formed over FTO/Poly-EDOT-C_{60}, the diffractogram (Fig. 7 bottom) shows the same peaks pattern observed for PS deposited over naked FTO, demonstrating that both films crystallized in the same single phase. The SEM and XRD results demonstrate that the presence of the Poly-EDOT-C_{60} layer does not affect the PS formation process, and that both PS films are formed over both substrates (FTO and FTO/Poly-EDOT-C_{60}) in the same way.

In order to investigate the ability of the Poly-EDOT-C_{60} films as electron extraction and transport layer, the steady-state photoluminescence (PL) of the PS films was studied. It can be seen from Fig. 8a (full lines) that FTO/Poly-EDOT-C_{60}/PS film as well as FTO/PS film present a PL band centered at around 765 nm. It is also evident that the PL of FTO/Poly-EDOT-C_{60}/PS film is quenched in 85% respect to the PL of FTO/PS film. The PL quenching effect by the different FTO/Poly-EDOT-C_{60} films is very similar for all of them, independently of the Poly-EDOT-C_{60} thickness. Moreover, irradiation of the films for 3 min leads to an increase (around two times) in the PL of FTO/PS film, but the PL of FTO/Poly-EDOT-C_{60}/PS films are not altered after the illumination process (Fig. 8a dotted lines). The quenching effect can be attributed to an efficient charge transfer between the PS and Poly-EDOT-C_{60} layers. The process is explained taking into account the energies of Poly-EDOT-C_{60} LUMO (obtained using the redox reduction potential of Poly-EDOT-C_{60} [48]) and perovskite conduction band. The correct alignment makes energetically possible the electron transfer from the perovskite conduction band to the Poly-EDOT-C_{60} layer (see diagram in Fig. 8b). This result indicates that Poly-EDOT-C_{60} films can be used as selective electron extraction and transport layer in PS solar cells.

3.5. Photovoltaic characterization

Fig. 9 shows the J-V response after different illumination times of a solar cell device with a Poly-EDOT-C_{60} layer obtained by one polymerization cycle. Before light exposure fresh devices present very low performance with the following photovoltaic parameters: open circuit potential (V_{oc}) of 554 mV, short circuit current (J_{sc}) of 13.7 mA/cm^2 and Fill Factor (FF) of 43%, and power conversion efficiency (PCE) of 3.3%. Interestingly, the performance of the device progressively increases with the illumination time until all the photovoltaic parameters reach almost constant values after five minutes of light soaking, even more, J-V curves taken at 30, 60 and 120 min practically fully overlap. However, during the five first minutes under illumination, the Voc and the FF are the two most affected parameters, increasing the PCE to 8.0% (V_{oc} = 875 mV, J_{sc} = 14.54 mA/cm^2, FF = 62.7%). The results above clearly show that activation of the ETL is required by light soaking treatment leading to important improvement of the performance with illumination. This effect has been observed previously for some perovskite devices and has been attributed to different causes, which may not be related to our case of study due to the novelty of our new system.

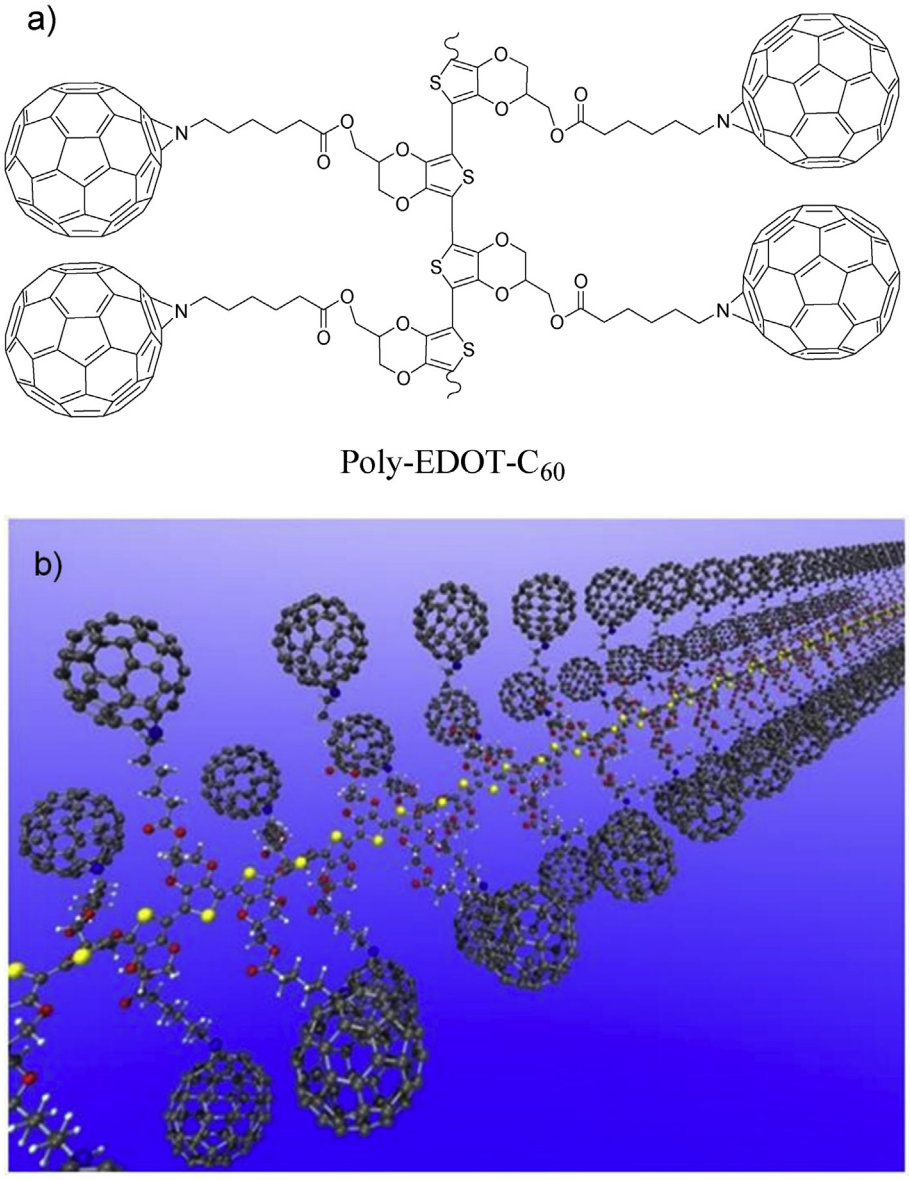

Fig. 5. a) Proposed structure of Poly-EDOT-C_{60} polymer. b) Three dimensional structure of Poly-EDOT-C_{60}.

For example, Shao et al. reported the use of a fullerene derivative with a high dielectric constant which suppressed both, the trap assisted recombination at interface between the perovskite and the C_{60}, and the light soaking effect [49]. It has also been proposed by Zhao et al. that the photogenerated charges neutralize the charges localized at the electrode interface, increasing the Voc and FF [50]. In both studies they used an inverted configuration where the C_{60} layer was spin coated over the perovskite. The surface traps in TiO_2 electron transport layer have also been the cause of the light soaking [51,52]. In our system this layer is not present and we propose that during the light soaking experiments ions are penetrating into the organic layer increasing the conductivity of the layer and reducing its resistance and recombination processes. This would be in good agreement with different proves that suggest that iodine ions migrate to the contacts under the effect of light and applied bias [53–55].

The effect of the light soaking and stability of the devices were studied as a function of the Poly-EDOT-C_{60} layer thickness (different number of polymerization cycles) as it is shown in Fig. 10a. Except for the device constructed with a Poly-EDOT-C_{60} layer of five polymerization cycles which presents an increase in PCE% after three days and a very small decrease after thirteen days (but still higher than the first day), the remaining devices present continuous increases in the PCE% after three and thirteen days of dark storage and test. The rise in PCE% for solar cells with two, three, and four Poly-EDOT-C_{60} polymerization cycles is principally due to a growth in the J_{sc} and FF values, since the V_{oc} slightly changes during the thirteen days (largest change is 10%). In the case of the device with five polymerization cycles the decrease in PCE% between three and thirteen days is because of a reduction in the FF. The lack of a trend is probably related with the variability of kinetics in ions penetrating into the Poly-EDOT-C_{60} layer, but in all cases the results clearly demonstrate that devices present adequate stability over the time.

In order to demonstrate the effect of the Poly-EDOT-C_{60} layer as electron transport layer in perovskite solar cells, reference devices

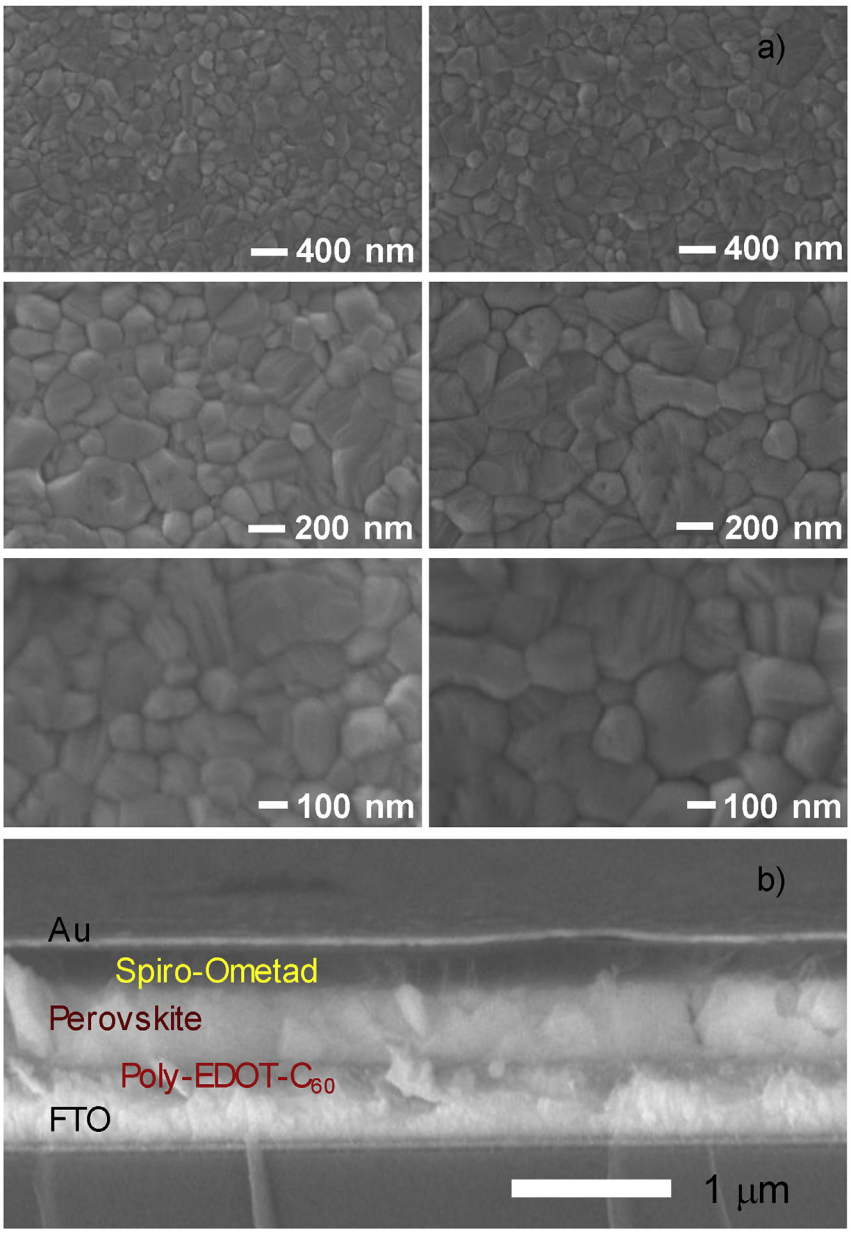

Fig. 6. a) Top view SEM images of PS films deposited over FTO (left), and over a FTO/Poly-EDOT-C_{60} layer with five polymerization cycles (right). b) Cross sectional SEM image showing the device architecture.

without a Poly-EDOT-C_{60} layer were also fabricated. Fig. 10b shows stabilized efficiency of the best devices after 13 days as a function of the number of polymerization cycles of Poly-EDOT-C_{60} layer. All devices with a Poly-EDOT-C_{60} layer present higher photovoltaic parameter values than the cell without a polymer layer. The PCE % for cells with Poly-EDOT-C_{60} layers obtained by one, two, three, and four, polymerization cycles, after thirteen days, are 9.5, 11.0, 9.0, and 10.0% respectively. All these values are similar and remarkably higher than the cells without Poly-EDOT-C_{60} layer, which typically lead to devices with very low efficiency (average values of ~3%). This result is in agreement with the observed perovskite PL quenching by the Poly-EDOT-C_{60} layer. However the cell with five polymerization cycles presents a low PCE % (6.1%) but still higher than the cell without Poly-EDOT-C_{60} layer. As it is shown in Fig. 10a, the low PCE % for the cell with 5 polymerization cycles is mainly due to the low FF % that could be associated to a high resistance of the polymeric film that requires very thin layers.

Therefore, the beneficial effect of the Poly-EDOT-C_{60} layer as electron selective contact in perovskite solar cells is clearly demonstrated. Further improvements in the device performances are possible by optimization of the ETL formation conditions, like monomer concentration, support electrolyte and/or electrochemical deposition method. In addition, modification in the monomers structure is possible and may lead to significant efficiency improvements.

4. Conclusions

In summary, a new C_{60} derivative monomer was designed, synthesized and polymerized on FTO electrodes. The Poly-EDOT-

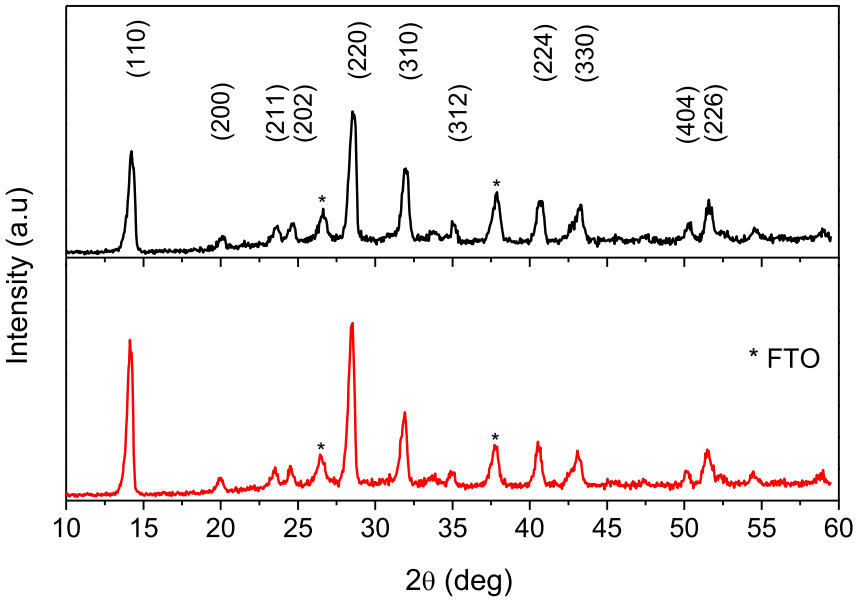

Fig. 7. X-ray diffractograms of $CH_3NH_3PbI_3$ perovskite layers deposited over FTO (top), and over a FTO/Poly-EDOT-C_{60} layer with five polymerization cycles (bottom). (The FTO peaks are marked with black asterisks).

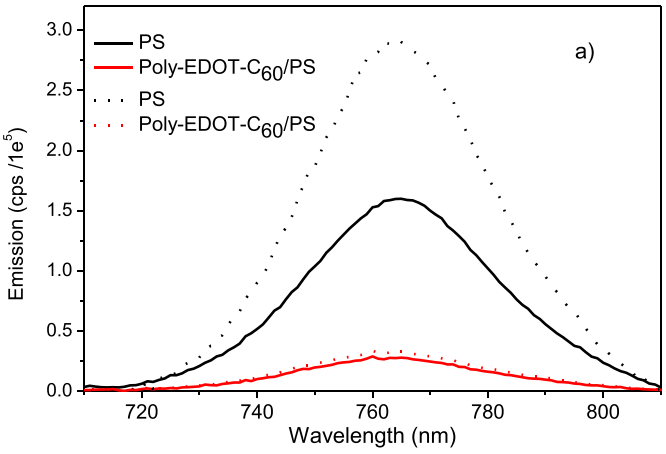

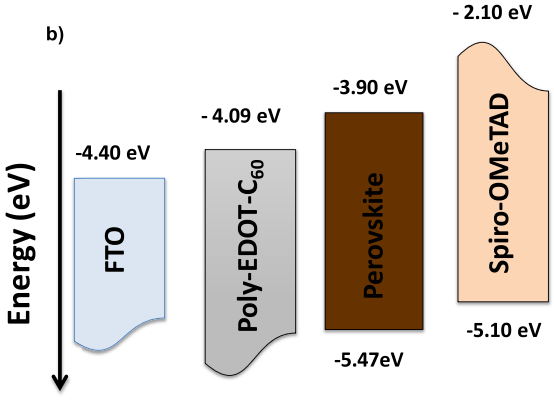

Fig. 8. a) Photoluminescence spectra of PS films deposited over FTO and over FTO/Poly-EDOT-C_{60} layers, before (full lines) and after (dotted lines) irradiation for 3 min. b) Schematic diagram of energy levels of the device.

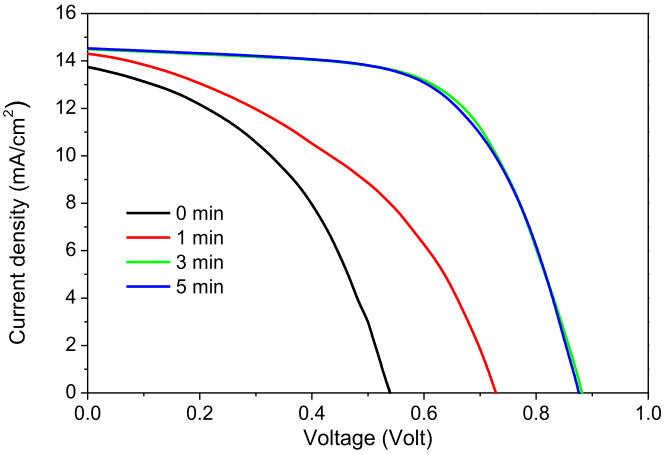

Fig. 9. J-V characteristics under after zero, one, three, and five illumination minutes of a device with a Poly-EDOT-C_{60} layer obtained by one polymerization cycle.

C_{60} electropolymeric films were easily obtained by a simple electrochemical methodology in one single step, avoiding the use of high temperatures which are employed in the formation of TiO_2 layers. Films were very smooth, conformal with the FTO substrate, highly transparent and were obtained with accurate thickness control. $CH_3NH_3PbI_3$ perovskite crystals were successfully grown over the electropolymeric films and their light emission was quenched by the presence of the organic polymer. Solar cells were constructed with the configuration FTO/Poly-EDOT-C_{60}/PS/spiro-OMeTAD/Au, which showed light soaking effects, reaching constant photovoltaic parameters after five illumination minutes. Measurements carried out as a function of the time showed that the efficiency evolves with time increasing to nearly stable values after thirteen days. Best devices exhibited an energy conversion efficiency of 11.0%, around four times higher than cells without Poly-EDOT-C_{60} layer. These results demonstrated that the use of a simple electrochemical methodology in the formation of organic electron transport layers as replacement of metal oxides in perovskite solar

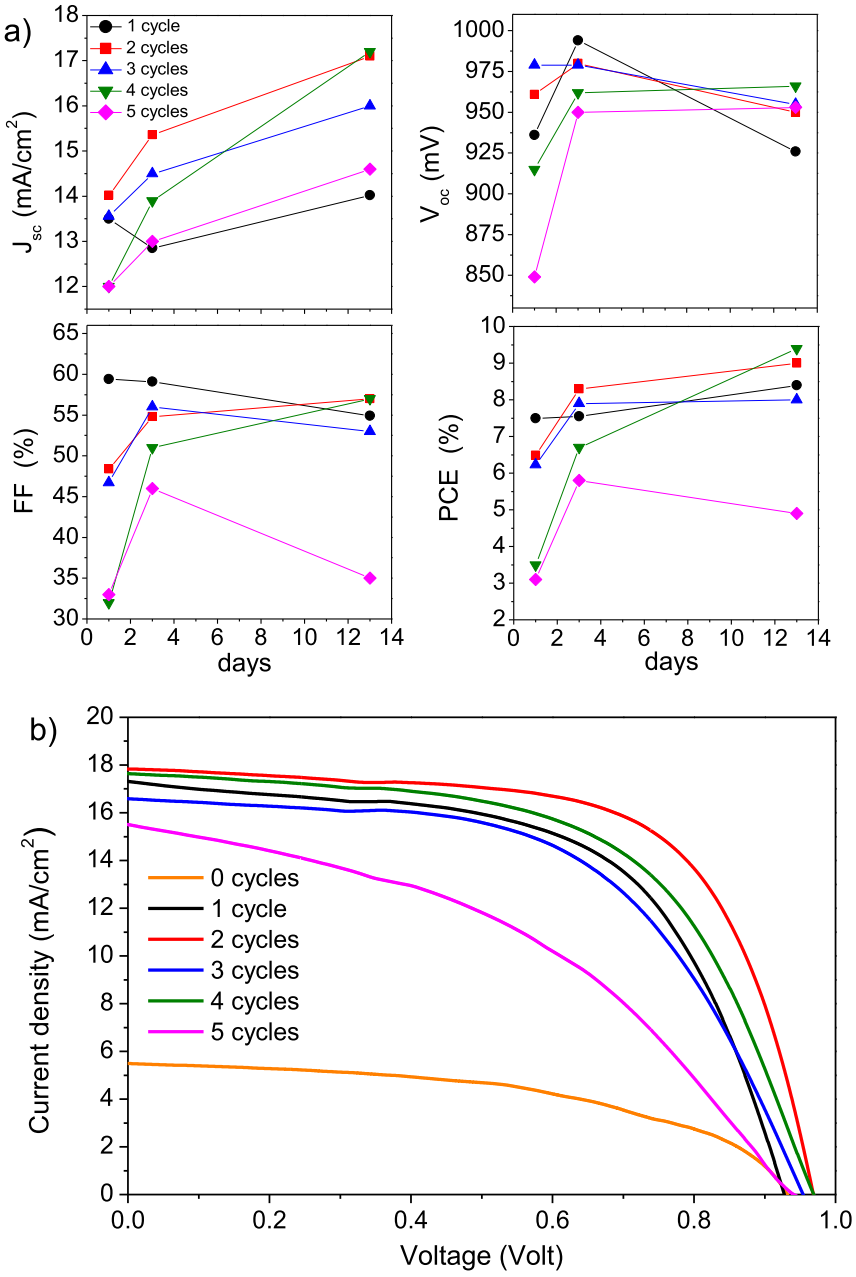

Fig. 10. Photovoltaic parameters (of five averaged devices), measured at different days, of devices with a Poly-EDOT-C_{60} layer obtained by one, two, three, four, and five polymerization cycles. b) J-V characteristics of the best devices with a Poly-EDOT-C_{60} layer obtained by one, two, three, four, and five polymerization cycles, and without a Poly-EDOT-C_{60} layer, after thirteen days.

cells opens a new approach in the fabrication of efficient energy conversion systems.

Acknowledgements

Authors are grateful to Secretaría de Ciencia y Técnica, Universidad Nacional de Río Cuarto (Secyt-UNRC), Consejo Nacional de Investigaciones Científicas y Técnicas (CONICET) and Agencia Nacional de Promoción Científica y Tecnológica (ANPCyT) of Argentina for financial support. L.M., J.D., D.H., E.N.D., L.O., and M.G., are Scientific Members of CONICET. M.B.S. thanks to CONICET, for postdoctoral fellowship. We thank financial support by Ministerio de Economía y Competitividad (MINECO) of Spain under project (MAT2016-76892-C3-1-R), and Universitat Jaume I for financial support on the project (UJI-B2017-32). A.G. would like to thank the MINECO for a Ramón y Cajal Fellowship (RYC-2014-16809).

References

[1] A. Kojima, K. Teshima, Y. Shirai, T. Miyasaka, Organometal halide perovskites as visible-light sensitizers for photovoltaic cells, J. Am. Chem. Soc. 131 (2009) 6050–6051.
[2] H. Chen, S. Xiang, W. Li, H. Liu, L. Zhu, S. Yang, Inorganic perovskite solar cells: a rapidly growing field, Sol. RRL 2 (2018) 1700188.
[3] M. Grätzel, The rise of highly efficient and stable perovskite solar cells, Acc. Chem. Res. 50 (2017) 487–491.
[4] Y. Chen, L. Zhang, Y. Zhang, H. Gaoa, H. Yan, Large-area perovskite solar cells–a review of recent progress and issues, RSC Adv. 8 (2018) 10489–10508.
[5] F. De Angelis, P. Kamat, Riding the New wave of perovskites, ACS Energy Lett. 2 (2017) 922–923.
[6] T. Xu, L. Chen, Z. Guo, T. Ma, Strategic improvement of the long-term stability

of perovskite materials and perovskite solar cells, Phys. Chem. Chem. Phys. 18 (2016) 27026–27050.
[7] H.S. Kim, C.R. Lee, J.H. Im, K.B. Lee, T. Moehl, A. Marchioro, S.J. Moon, R. Humphry-Baker, J.H. Yum, J.E. Moser, M. Grätzel, N.G. Park, Lead iodide perovskite sensitized all-solid-state submicron thin film mesoscopic solar cell with efficiency exceeding 9%, Sci. Rep. 2 (2012) 591.
[8] M.M. Lee, J. Teuscher, T. Miyasaka, T.N. Murakami, H.J. Snaith, Efficient hybrid solar cells based on meso-superstructured organometal halide perovskites, Science 338 (2012) 643.
[9] W. Ke, G. Fang, Q. Liu, L. Xiong, P. Qin, H. Tao, J. Wang, H. Lei, B. Li, J. Wan, Low-temperature solution-processed tin oxide as an alternative electron transporting layer for efficient perovskite solar cells, J. Am. Chem. Soc. 137 (2015) 6730–6733.
[10] D. Liu, T.L. Kelly, Perovskite solar cells with a planar heterojunction structure prepared using room-temperature solution processing techniques, Nat. Photon. 8 (2013) 133–138.
[11] J.M. Ball, M.M. Lee, A. Hey, H.J. Snaith, Low-temperature processed meso-superstructured to thin-film perovskite solar cells, Energy Environ. Sci. 6 (2013) 1739–1743.
[12] J.Y. Jeng, Y.F. Chiang, M.H. Lee, S.R. Peng, T.F. Guo, P. Chen, T.C. Wen, $CH_3NH_3PbI_3$ Perovskite/fullerene planar-heterojunction hybrid solar cells, Adv. Mater. 25 (2013) 3727–3732.
[13] W. Yin, L. Pan, T. Yang, Y. Liang, Recent advances in interface engineering for planar heterojunction perovskite solar cells, Molecules 21 (2016) 837.
[14] Y. Bai, X. Meng, S. Yang, Interface engineering for highly efficient and stable planar p-i-n perovskite solar cells, Adv. Energy Mater. 8 (2018), 1701883.
[15] J. You, Z. Hong, Y.M. Yang, Q. Chen, M. Cai, T.-B. Song, C.-C. Chen, S. Lu, Y. Liu, H. Zhou, Y. Yang, Low-temperature solution-processed perovskite solar cells with high efficiency and flexibility, ACS Nano 8 (2014) 1674–1680.
[16] Y. Fang, C. Bi, D. Wang, J. Huang, The functions of fullerenes in hybrid perovskite solar cells, ACS Energy Lett. 2 (2017) 782–794.
[17] D. Liu, Q. Wang, Ch. J. Traverse, C. Yang, M. Young, P.S. Kuttipillai, S.Y. Lunt, Th.W. Hamann, R.R. Lunt, Impact of ultrathin C_{60} on perovskite photovoltaic devices, ACS Nano 12 (2018) 876–883.
[18] C. Tian, E. Castro, G. Betancourt-Solis, Z. Nan, O. Fernandez-Delgado, S. Jankurua, L. Echegoyen, Fullerene derivative with a branched alkyl chain exhibits enhanced charge extraction and stability in inverted planar perovskite solar cells, New J. Chem. 42 (2018) 2896–2902.
[19] K. Wojciechowski, I. Ramirez, T. Gorisse, O. Dautel, R. Dasari, N. Sakai, J. Martinez Hardigree, S. Song, S. Marder, M. Riede, G. Wantz, H.J. Snaith, Cross-linkable fullerene derivatives for solution-processed n–i–p perovskite solar cells, ACS Energy Lett. 1 (2016) 648–653.
[20] M. Valles-Pelarda, B. Clasen Hames, I. García-Benito, O. Almora, A. Molina-Ontoria, R.S. Sanchez, G. Garcia-Belmonte, N. Martín, I. Mora-Sero, Analysis of the Hysteresis behavior of perovskite solar cells with interfacial fullerene self-assembled monolayers, J. Phys. Chem. Lett. 7 (2016) 4622–4628.
[21] Y. Shao, Z. Xiao, C. Bi, Y. Yuan, J. Huang, Origin and elimination of photocurrent hysteresis by fullerene passivation in $CH_3NH_3PbI_3$ planar heterojunction solar cells, Nat. Commun. 5 (2014) 5784.
[22] L. Kegelmann, C.M. Wolff, C. Awino, F. Lang, E.L. Unger, L. Korte, T. Dittrich, D. Neher, B. Rech, S. Albrecht, It takes two to tango—double-layer selective contacts in perovskite solar cells for improved device performance and reduced hysteresis, ACS Appl. Mater. Interfaces 9 (2017) 17245–17255.
[23] C. Tao, S. Neutzner, L. Colella, S. Marras, A.R. Srimath Kandada, M. Gandini, M.D. Bastiani, G. Pace, L. Manna, M. Caironi, 17.6% stabilized efficiency in low-temperature processed planar perovskite solar cells, Energy Environ. Sci. 8 (2015) 2365–2370.
[24] Y. Zhong, R. Munir, A.H. Balawi, A.D. Sheikh, L. Yu, M.-C. Tang, H. Hu, F. Laquai, A. Amassian, Mesostructured fullerene electrodes for highly efficient n–i–p perovskite solar cells, ACS Energy Lett. 1 (2016) 1049–1056.
[25] A. Guerrero, G. Garcia-Belmonte, Recent advances to understand morphology stability of organic photovoltaics, Nano-Micro Lett. 9 (2016) 10.
[26] W. Yan, Y. Li, Y. Li, S. Ye, Z. Liu, S. Wang, Z. Bian, C. Huang, High-performance hybrid perovskite solar cells with open circuit voltage dependence on hole-transporting materials, Nano Energy 16 (2015) 428–437.
[27] W. Yan, Y. Li, Y. Li, S. Ye, Z. Liu, S. Wang, Z. Bian, C. Huang, Stable high-performance hybrid perovskite solar cells with ultrathin polythiophene as hole-transporting layer, Nano Res. 8 (2015) 2474–2480.
[28] C. Solis, M.B. Ballatore, M.B. Suarez, M.E. Milanesio, E.N. Durantini, M. Santo, Th. Dittrich, L. Otero, M. Gervaldo, Electrochemical generation of a molecular heterojunction. A new zn-porphyrin-fullerene C_{60} polymeric film, Electrochim. Acta 238 (2017) 81–90.
[29] M. Gervaldo, P.A. Liddell, G. Kodis, B.J. Brennan, C.R. Johnson, J.W. Bridgewater, A.L. Moore, T.A. Moore, D.A. Gust, A photo- and electrochemically-active porphyrin-fullerene dyad electropolymer, Photochem. Photobiol. Sci. 9 (2010) 890–900.
[30] M. Otero, T. Dittrich, J. Rappich, D. Heredia, F. Fungo, E. Durantini, L. Otero, Photoinduced charge separation in organic-inorganic hybrid system: C60-containing electropolymer/CdSe-quantum dots, Electrochim. Acta 173 (2015) 316–322.
[31] T.A. Halgren, MMFF VI. MMFF94s option for energy minimization studies, J. Comput. Chem. 20 (1999) 720–729.
[32] M.D. Hanwell, D.E. Curtis, D.C. Lonie, T. Vandermeersch, E. Zurek, G.R. Hutchison, Avogadro: an advanced semantic chemical editor, visualization, and analysis platform, J. Cheminf. 4 (2012) 1–17.
[33] J. Durantini, M.B. Suarez, M. Santo, E. Durantini, T. Dittrich, L. Otero, M. Gervaldo, Photoinduced charge separation in organic–organic heterojunctions based on porphyrin electropolymers. Spectral and time dependent surface photovoltage study, J. Phys. Chem. C 119 (2015) 4044–4051.
[34] C. Solis, E. Baigorria, M.E. Milanesio, G. Morales, E.N. Durantini, L. Otero, M. Gervaldo, Electrochemical polymerization of EDOT modified Phthalocyanines and their applications as electrochromic materials with green coloration, and strong absorption in the Near-IR, Electrochim. Acta 213 (2016) 594–605.
[35] E. Nasybulin, S. Wei, M. Cox, I. Kymissis, K. Levon, Morphological and spectroscopic studies of electrochemically deposited poly(3,4-ethylenedioxythiophene) (PEDOT) hole extraction layer for organic photovoltaic device (OPVD) fabrication, J. Phys. Chem. C 115 (2011) 4307–4314.
[36] A.J. Bard, L.R. Faulkner, Electrochemical Methods. Fundamentals and Applications, second ed., vol. 13, Wiley-VCH-, 2001, pp. 580–601.
[37] J. Durantini, L. Otero, M. Funes, E.N. Durantini, F. Fungo, M. Gervaldo, Electrochemical oxidation-induced polymerization of 5,10,15,20-tetrakis[3-(*N*-ethylcarbazoyl)]porphyrin. Formation and characterization of a novel electroactive porphyrin thin film, Electrochim. Acta 56 (2011) 4126–4134.
[38] M. Gervaldo, M. Funes, J. Durantini, L. Fernandez, F. Fungo, L. Otero, Electrochemical polymerization of Palladium (II) and free base 5,10,15,20-tetrakis(4-N,N-diphenylaminophenyl)porphyrins: its applications as electrochromic and photoelectric materials, Electrochim. Acta 55 (2010) 1948–1957.
[39] W. Yan, Y. Li, W. Sun, H. Peng, S. Ye, Z. Liu, Z. Bian, C. Huang, High-performance hybrid perovskite solar cells with polythiophene as hole-transporting layer via electrochemical polymerization, RSC Adv. 4 (2014) 33039–33046.
[40] M.C. Fravventura, J. Hwang, J.W.A. Suijkerbuijk, P. Erk, L.D.A. Siebbeles, T.J. Savenije, Determination of singlet exciton diffusion length in thin evaporated C_{60} films for photovoltaics, J. Phys. Chem. Lett. 3 (2012) 2367–2373.
[41] V. Capozzi, G. Casamassima, G.F. Lorusso, A. Minafra, R. Piccolo, T. Trovato, A. Valentini, Optical spectra and photoluminescence of C_{60} thin films, Solid State Commun. 98 (1996) 853–858.
[42] F. Negri, G. Orlandi, F. Zerbetto, Interpretation of the vibrational structure of the emission and absorption spectra of C_{60}, J. Chem. Phys. 97 (1992) 6496–6503.
[43] J.H. Noh, S.H. Im, J.H. Heo, T.N. Mandal, S.I. Seok, Chemical management for colorful, efficient, and stable inorganic–organic hybrid nanostructured solar cells, Nano Lett. 13 (2013) 1764–1769.
[44] B. Suarez, V. Gonzalez-Pedro, T.S. Ripolles, R.S. Sanchez, L. Otero, I. Mora-Sero, Recombination study of combined halides (Cl, Br, I) perovskite solar cells, J. Phys. Chem. Lett. 5 (2014) 1628–1635.
[45] W. Yan, Y. Li, S. Ye, Y. Li, H. Rao, Z. Liu, S. Wang, Z. Bian, C. Huang, Increasing open circuit voltage by adjusting work function of hole-transporting materials in perovskite solar cells, Nano Res. 9 (2016) 1600–1608.
[46] G. Murugadoss, H. Kanda, S. Tanaka, H. Nishino, S. Ito, H. Imahori, T. Umeyama, An efficient electron transport material of tin oxide for planar structure perovskite solar cells, J. Power Sources 307 (2016) 891–897.
[47] T. Baikie, Y. Fang, J.M. Kadro, M. Schreyer, F. Wei, S.G. Mhaisalkar, M. Gratzel, T.J. White, Synthesis and crystal chemistry of the hybrid perovskite $CH_3NH_3PbI_3$ for solid-state sensitised solar cell applications, J. Mater. Chem. A 1 (2013) 5628–5641.
[48] N. Ahn, D.-Y. Son, I.-H. Jang, S.M. Kang, M. Choi, N.-G. Park, Highly reproducible perovskite solar cells with average efficiency of 18.3% and best efficiency of 19.7% fabricated via Lewis base adduct of lead(II) iodide, J. Am. Chem. Soc. 137 (2015) 8696–8699.
[49] S. Shao, M. Abdu-Aguye, L. Qiu, L.-H. Lai, J. Liu, S. Adjokatse, F. Jahani, M.E. Kamminga, G.H. ten Brink, T.T.M. Palstra, B.J. Kooi, J.C. Hummelen, M.A. Loi, Elimination of the light soaking effect and performance enhancement in perovskite solar cells using a fullerene derivative, Energy Environ. Sci. 9 (2016) 2444–2452.
[50] C. Zhao, B. Chen, X. Qiao, L. Luan, K. Lu, B. Hu, Perovskite solar cells: revealing underlying processes involved in light soaking effects and hysteresis phenomena in perovskite solar cells, Adv. Energy Mater. 5 (2015), 1500279.
[51] Y. Li, Y. Zhao, Q. Chen, Y. (Michael) Yang, Y. Liu, Z. Hong, Z. Liu, Y.-T. Hsieh, L. Meng, Y. Li, Y. Yang, Multifunctional fullerene derivative for interface engineering in perovskite solar cells, J. Am. Chem. Soc. 137 (2015) 15540–15547.
[52] J.H. Heo, M.S. You, M.H. Chang, W. Yin, T.K. Ahn, S.-J. Lee, S.-J. Sung, D.-H. Kim, S.-H. Im, Hysteresis-less mesoscopic $CH_3NH_3PbI_3$ perovskite hybrid solar cells by introduction of Li-treated TiO_2 electrode, Nano Energy 15 (2015) 530–539.
[53] R. Gottesman, P. Lopez-Varo, L. Gouda, J.A. Jimenez-Tejada, J. Hu, S. Tirosh, A. Zaban, J. Bisquert, Dynamic phenomena at perovskite/electron-selective contact interface as interpreted from photovoltage decays, Chem 1 (2016) 776–789.
[54] A. Guerrero, J. You, C. Aranda, Y.S. Kang, G. Garcia-Belmonte, H. Zhou, J. Bisquert, Y. Yang, Interfacial degradation of planar lead halide perovskite solar cells, ACS Nano 10 (2016) 218–224.
[55] J. Carrillo, A. Guerrero, S. Rahimnejad, O. Almora, I. Zarazua, E. Mas-Marza, J. Bisquert, G. Garcia-Belmonte, Ionic reactivity at contacts and aging of methylammonium lead triiodide perovskite solar cells, Adv. Energy Mater. 6 (2016) 1502246.